

Electronic Supplementary Information (ESI)

Hydrotalcite based Ni-Fe/(Mg, Al)O_x catalysts for CO₂ methanation – tailoring Fe content for improved CO dissociation, basicity, and particle size

C. Mebrahtu,^{a,b} F. Krebs,^{b,c} S. Perathoner,^a S. Abate,^a G. Centi,^a and R. Palkovits^{b,c*}

The synthesis strategy via hydrotalcite provides materials with interesting properties after calcination covering high BET surface area, tailored acid/base properties, homogeneous mixtures of oxides with very small crystal size and thermal stability.

He et al. (2014) reported a Ni-Al hydrotalcite derived catalyst (Ni-Al₂O₃-HT) which exhibited a narrow Ni particle-size distribution with an average particle size of 4.0 nm. Methanation of CO₂ over this catalyst initiated at 225°C and reached 82.5% CO₂ conversion with 99.5% CH₄ selectivity at 350°C, significantly outperforming a catalyst of the comparable composition prepared via impregnation. The existence of strong basic sites facilitated the activation of CO₂ and consequently promoted the activity. The combination of highly dispersed Ni with a strong basic support led to its unique and high efficiency for this reaction.¹ Abello and coworkers also designed Ni-Al-HTs based catalysts with high Ni loadings by conventional co-precipitation. Despite the high nickel loading (70 wt.%), which is theoretically thought to be counterproductive for the catalytic performance of nickel-based catalysts, the Ni-Al activated catalyst exhibited high CO₂ conversion and rendered a CH₄ selectivity very close to 100% possible. This was attributed to the formation of small metallic nickel crystallites (ca. 6 nm) dispersed over NiO-alumina upon partial reduction of the mixed oxide.²

Herein, we propose hydrotalcite derived Ni-Fe bimetallic catalysts for CO₂ methanation with relatively low active metal content as higher active metal loadings potentially compromise the stability of the catalyst during long-term operation.³

Characterization Procedures

N₂-Physisorption

Specific surface area (Multipoint BET) and total pore volume of the calcined catalysts were determined by N₂ physisorption at -195.79°C using Quadrasorb SI Automated Surface Area and Pore Size Analyzer from Quantachrome Instruments after degassing the sample at 200°C for 20 h at a residual pressure of 0.352 mbar.

XRD

XRD measurements were performed for both the dried hydrotalcite precursors and calcined catalysts using a D5000 Siemens XRD diffractometer with a Cu K_α X-ray tube (λ = 1.54056 Å). The tube voltage and current were 45 kV and 40 mA, respectively. Diffraction patterns were collected in the 3-90° 2θ range.

ICP-OES

The chemical composition of the calcined catalysts was analyzed by inductively coupled plasma-optical emission spectroscopy (ICP-OES; Spectro Analytical Instruments). Prior to the analysis of metals (Ni, Mg, Fe, Al), 30 mg of each sample was dissolved in an acidic solution composed of 8 mL of HF, 2 mL of H₂SO₄ and 40 mL of demineralized water.

TGA-DSC

Thermogravimetric and differential scanning calorimetry (TGA-DSC) analyses of the dried hydrotalcite-like precursors were conducted in order to study the thermal decomposition properties in air using a Netzsch STA 409 apparatus. Samples were heated from 30°C to 900°C with a heating rate of 5°C/min in air.

H₂-TPR

Temperature programmed reduction (H₂-TPR) properties of the calcined catalysts were investigated using ChemBET Pulsar TPR/TPD/TPO (Quantachrome Instruments). Prior to the measurement, about 130 mg of sample was pretreated at 200°C for 1 h in He gas stream. The H₂-TPR profile was then recorded from room temperature to 1000°C with a heating ramp of

^a Dipartimento di Ingegneria, Università di Messina and INSTM CASPE (Laboratory of Catalysis for Sustainable Production and Energy) and ERIC- Viale F. Stagno D'Alcontres 31, 98165 Messina, Italy.

^b Lehrstuhl für Heterogene Katalyse und Technische Chemie, Institut für Technische und Makromolekulare Chemie (ITMC) RWTH Aachen University, Worringerweg 2, 52074 Aachen, Germany.

^c Competence Center Power to Fuel/RWTH Aachen University, Schinkelstraße 2, 52062 Aachen, Germany.

* Corresponding author: Palkovits@itmc.rwth-aachen.de

10°C/min under a flow of 5% H₂ in Ar with a flow rate of 100 mL/min.

Irreversible adsorption of organic acids

Basic sites of the calcined catalysts were determined using irreversible adsorption of organic acids. Acrylic acid ($pK_a = 4.3$) and phenol ($pK_a = 9.9$) were used as probe molecules to determine the content of total basic sites and strong basic sites, respectively.^{4, 5} The weak basic sites were then quantified by subtracting the concentration of strong basic sites from the content of total basic sites. The initial and final concentrations of the acids i.e. before and after adsorption experiment were measured spectrophotometrically (StellarNet Inc.) at wavelength 245 nm and 242 nm for acrylic acid and phenol, respectively.

STEM-EDS

STEM images and EDS analyses of selected catalysts after reduction were performed using TEM (JEOL JEM-2200FS) equipped with a slow scan CCD camera Gatan for high resolution (HR) TEM, a scanning transmission electron mode (STEM) and an energy dispersive X-ray (EDX) spectrometer.

CO₂-TPD

The CO₂ desorption experiments were performed on a (PROTEC TPDRO 1100 Series) analyzer with a TCD detector. Prior to analysis, the calcined hydrotalcite based catalyst (200 mg) was thermally treated under N₂ flow at 300°C for 1 h. Next, it was cooled down to room temperature for CO₂ adsorption (20 mL/min, 60 min) and then flushed with N₂ (20 mL/min, 10 min) at 50°C to eliminate physically adsorbed CO₂. Finally, TPD profiles were recorded under He stream (25 mL/min) with a heating rate of 10 °C/min up to 900°C.

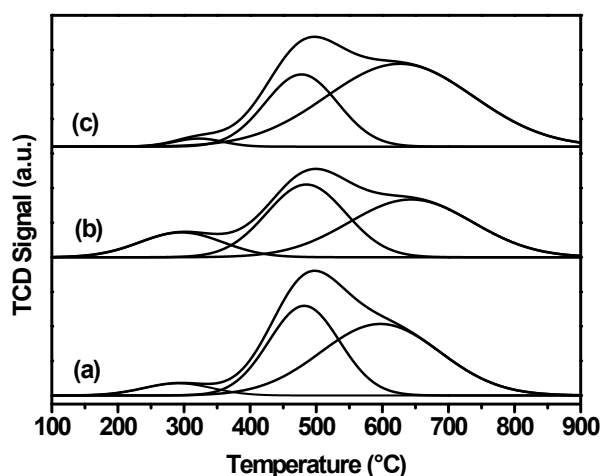


Figure S1 CO₂ TPD profiles: (a) Ni-Fe/Mg/Al (Fe/Ni = 0), (b) Ni-Fe/Mg/Al (Fe/Ni = 0.1) and (c) Ni-Fe/Mg/Al (Fe/Ni = 0.5).

Table S1 Integrated peak areas of basic sites with different strength.

Catalyst	Desorption Peak area (%)		
	L.T.P.	M.T.P.	H.T.P.
Ni/(Mg, Al)O _x	5	45	50
Ni-Fe/(Mg, Al)O _x (Fe/Ni=0.1)	14	31	55
Ni-Fe/(Mg, Al)O _x (Fe/Ni=0.5)	2	30	68

L.T.P = Low temperature peak, M.T.P = Medium temperature peak and H.T.P = High temperature peak

XPS

Chemical states of selected Ni-Fe/Mg/Al catalysts (reduced at 600°C) were determined by X-ray photoelectron spectroscopy. The XPS signals were collected using PHI VersaProbe II analyzer. Ni2p and Fe2p binding energies were recorded using AlK α (1486.6 eV) as the excitation source and a pass energy of 23.5 eV. The X-ray setting was 100 μ 100W20kV_HP. A Shirley background was applied and all the XPS peaks were fitted with asymmetric function by using the Multipeak software. The binding energies obtained in the XPS analysis were calibrated using C1s as a reference with binding energy equal to 284.8 eV.

Raman

Raman spectra were obtained using DXR Raman microscope with an exciting line of 532 nm and 2 mW power.

CO₂ TPD

The mixed oxide forms of selected hydrotalcite derived samples were analyzed by temperature programmed desorption (TPD) of CO₂, aiming to have an overview on the strength and distribution of basic sites on the surface of the catalysts. The corresponding CO₂ temperature-programmed desorption profiles (Figure S1) were deconvoluted in three desorption peaks, reaching maximum desorption rate in the temperature ranges of 290-324°C, 479-484°C, and 597-643°C. Di Cosimo *et al.* (1998) studying mixed oxides derived from hydrotalcites also observed that the TPD profiles could be deconvoluted in three peaks with different basic strength. The elementary peaks obtained from deconvolution of the whole temperature range TPD profile can be related to the origin of the basic sites as follow: lower temperature peak (low-strength basic sites) to surface hydroxyl groups and the medium temperature (medium strength basic sites) and higher temperature (high strength basic sites) peaks to surface basic oxygen atoms.⁶ The relative contribution of each desorption peak calculated by the integration of the respective profile is listed in Table S1. From the integrated peak areas, it can be observed that the Ni-Fe/Mg/Al (Fe/Ni = 0.1) catalyst has better amount of desorbed CO₂ in the low temperature region which can be advantageous for the methanation reaction.

XPS Analysis

The Ni2p signals for Ni-Fe/(Mg, Al)O_x (Fe/Ni = 0.1) and Ni-Fe/(Mg, Al)O_x (Fe/Ni = 0.5) catalysts appears at 855.85 eV and 855.7 eV with satellite peaks at 862.15 eV and 861.90 eV, respectively (Figure S2). The main peaks obtained were deconvoluted and mathematically treated to identify the chemical species of nickel present in the surface of the reduced catalysts. Accordingly, the smaller peak at around 852 eV was ascribed to the presence of Ni metal. The peaks at about 854.95-856 eV can be assigned to the NiO, Ni(OH)₂ and/or NiFe₂O₃ spinel species on the surface.^{7,8} Surface compositions for the Fe/Ni ratios were calculated from the wide scan XPS and results were found to be 0.08 and 0.43 for the Ni-Fe/(Mg, Al)O_x (Fe/Ni = 0.1) and Ni-Fe/(Mg, Al)O_x (Fe/Ni = 0.5) catalysts, respectively.

Furthermore, for Ni-Fe/(Mg, Al)O_x (Fe/Ni = 0.1) catalyst the signals due to Fe2p was very noisy and difficult to detect this might be due to the lower concentration of Fe on the surface. But for Ni-Fe/(Mg, Al)O_x (Fe/Ni = 0.5) catalyst, the Fe2p signal was detected and successfully traced as shown in Figure S3. The signals with binding energy equal to 711.5 eV and 724.6 eV are attributed to the oxidized state (Fe₂O₃) species of Fe.

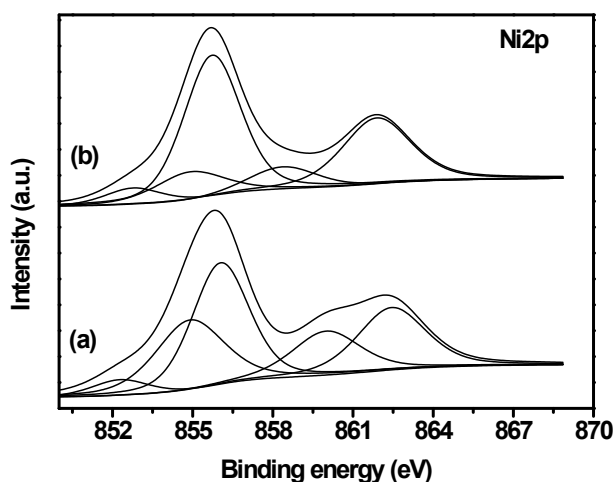


Figure S2 Ni2p XPS spectra: (a) Ni-Fe/(Mg, Al)O_x (Fe/Ni = 0.1) and (b) Ni-Fe/(Mg, Al)O_x (Fe/Ni = 0.5).

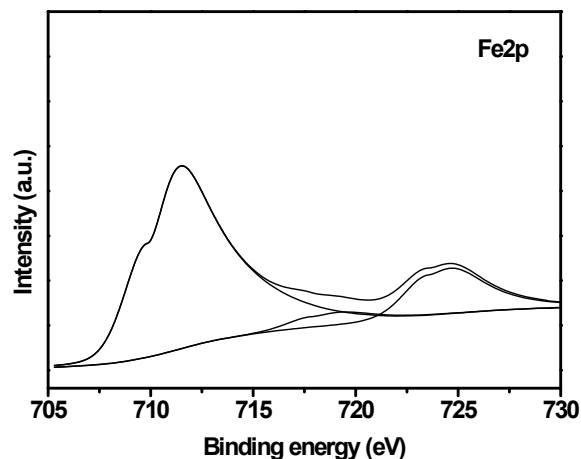


Figure S3 Fe2p XPS spectrum for Ni-Fe/Mg/Al (Fe/Ni = 0.5) catalyst.

STEM

The STEM dark field micrographs of the reduced catalysts (Figure S4) were used for the calculation of the average particle size referring to alloys formed after reduction. The calcined samples were reduced under similar conditions as used for the catalytic reaction at 600°C for 2 h in pure H₂.

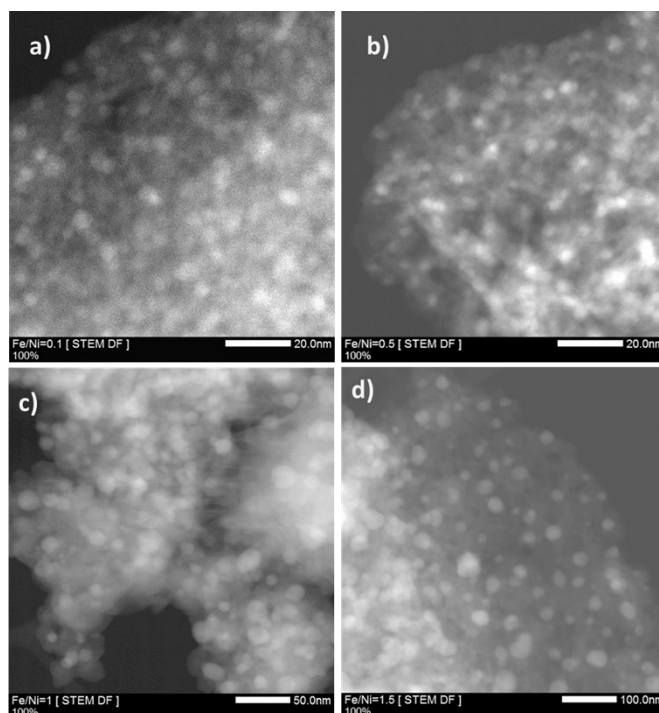


Figure S4 STEM images of reduced HTs derived bimetallic catalysts: a) Ni-Fe/(Mg, Al)O_x (Fe/Ni = 0.1), b) Ni-Fe/(Mg, Al)O_x (Fe/Ni = 0.5), c) Ni-Fe/(Mg, Al)O_x (Fe/Ni = 1) and d) Ni-Fe/(Mg, Al)O_x (Fe/Ni = 1.5).

Raman

Raman measurements were performed to evaluate the effect of iron promoting the formation of either forming Fe_3O_4 or spinel (Figure S5).

TGA-DSC

The decomposition profiles of catalysts with higher Fe content i.e. $\text{Ni-Fe}/(\text{Mg, Al})\text{O}_x$ ($\text{Fe}/\text{Ni} = 1.5$) and $\text{Fe}/\text{Mg}/\text{Al}$ samples slightly differs from the other three samples, in both catalysts the lower and higher temperature regions exhibited additional features, where various small transitions can be observed. The decomposition takes place in four steps at 100°C (removal of physisorbed water), 265°C (removal of interlayer water) and 351°C (dehydroxylation and decarbonation). A broad peak at higher temperature (ca. 652°C) in the DSC plot can be assigned

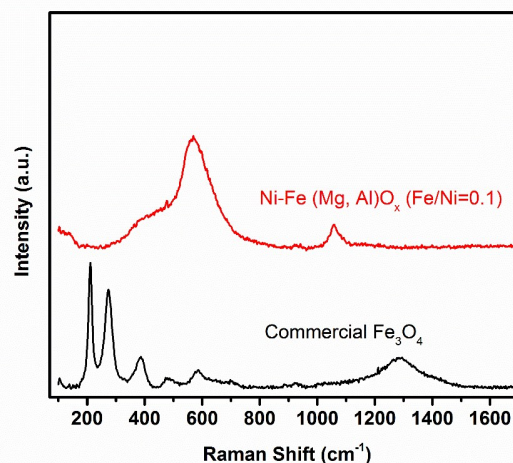


Figure S5 Raman spectra of commercial Fe_3O_4 and calcined $\text{Ni-Fe}/(\text{Mg, Al})\text{O}_x$ ($\text{Fe}/\text{Ni} = 0.1$) HTs catalyst.

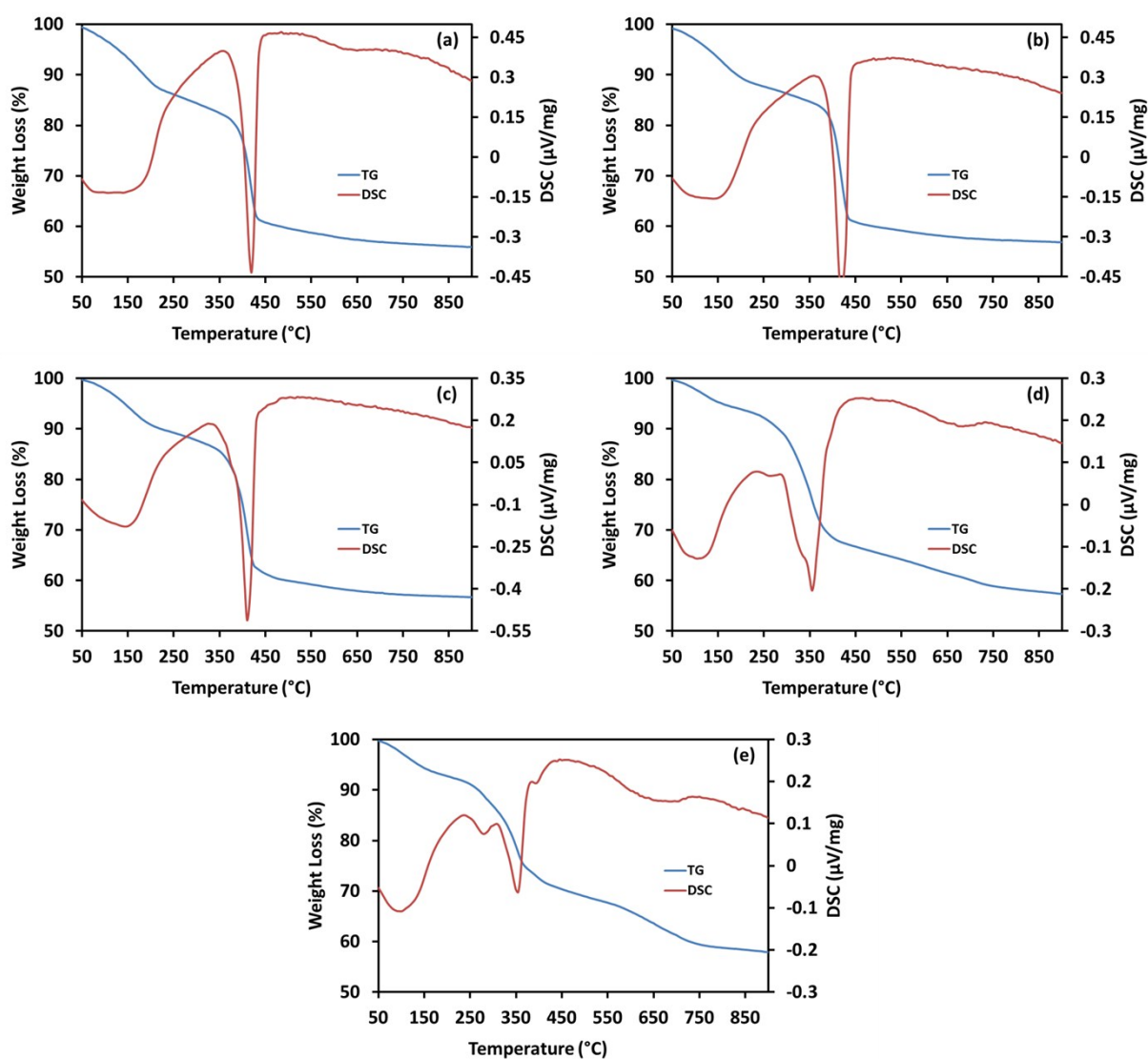


Figure S6 Representative TGA-DSC curves of the dried precursors: a) $\text{Ni}/(\text{Mg, Al})\text{O}_x$, b) $\text{Ni-Fe}/(\text{Mg, Al})\text{O}_x$ ($\text{Fe}/\text{Ni} = 0.1$), c) $\text{Ni-Fe}/(\text{Mg, Al})\text{O}_x$ ($\text{Fe}/\text{Ni} = 0.5$), d) $\text{Ni-Fe}/(\text{Mg, Al})\text{O}_x$ ($\text{Fe}/\text{Ni} = 1.5$) and e) $\text{Fe}/(\text{Mg, Al})\text{O}_x$.

to a fourth step. As stated elsewhere,⁹ this might be due to delayed crystallization of ferrite species (takes place at higher temperatures) when iron exists in the interlayer, instead of in the hydroxide layers.

Post reaction characterizations

XRD analysis of spent catalysts

XRD analysis of selected spent catalysts was performed to investigate the Ni-Fe alloy formation during reaction after the in-situ reduction (Figure S7). The diffraction patterns of catalysts after the CO₂ methanation have the periclase support in common. For the samples after reaction reflexes from NaNO₃ could not be detected anymore, that concludes all left nitrates decomposed most probably due to the in situ reduction at 600°C prior to the reaction. In addition, ICP measurements showed no distinct correlation between the sodium concentration and activity. Therefore we conclude that the lower concentration sodium incorporated in phases was not affected the performance of the catalysts towards CO₂ methanation.

Taking a closer look at the d(200) value for reflections at around $2\theta \approx 51^\circ$ it is possible to study formation of alloy during the reaction by applying Vegard's law. Based on the calculated d-spacing values for catalysts with lower (Fe/Ni = 0.1) and higher (Fe/Ni = 0.5) iron content there is an evidence for an alloy formation because the values obtained are in between the theoretical values compared to pure elements and follow along Vegard's law (Figure S8). The data shows a good linear correlation, as Vegard's law is not exact; a perfect correlation is not expected. The formation of Ni-Fe alloys was also confirmed from TEM-EDS measurements. The values for fcc Ni metal = 0.1762 nm (JCPDS 01-070-1849) and fcc γ -Fe = 0.1823 nm (JCPDS 01-089-4185) were taken to plot the correlation curve.

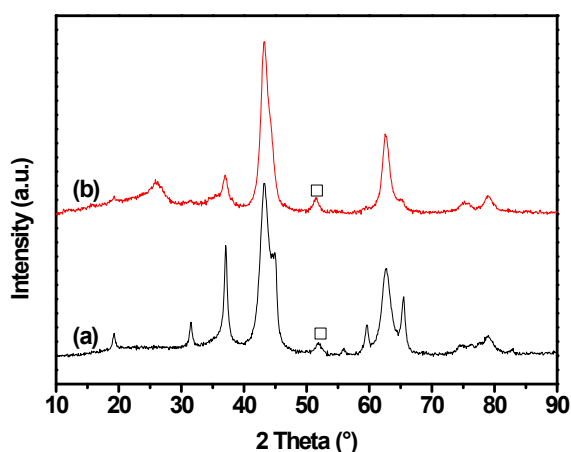


Figure S7 XRD pattern of the catalysts after the CO₂ methanation (a) Ni-Fe/(Mg, Al)O_x (Fe/Ni = 0.1) and (b) Ni-Fe/(Mg, Al)O_x (Fe/Ni = 0.5): formation of Ni-Fe alloys (□).

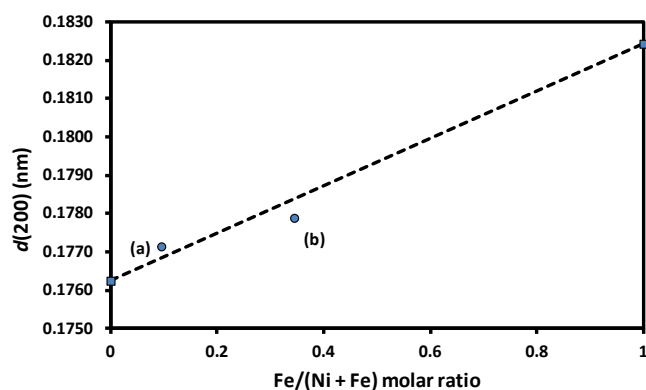


Figure S8 XRD Dependence of d(200) spacing for Fe-Ni alloys as a function of the Fe/(Ni + Fe) molar ratio for catalysts after CO₂ methanation: (a) Ni-Fe/(Mg, Al)O_x (Fe/Ni = 0.1) and (b) Ni-Fe/(Mg, Al)O_x (Fe/Ni = 0.5). The dashed line describes theoretical behavior using Vegard's law with fcc Ni metal (JCPDS 01-070-1849) and fcc γ -Fe (JCPDS 01-089-4185) as references (■).

TG analysis of spent catalyst

Carbon deposition behavior of the Ni-Fe/(Mg, Al)O_x (Fe/Ni = 0.1) catalyst after 24 h reaction was evaluated by TG analysis under air atmosphere. From a typical TGA profile of a sample with deposited carbon, weight loss at temperature between 400°C to 500°C can be assigned to the removal of easily oxidizable amorphous carbon and the weight loss at above 500°C is attributed to the oxidation of a graphitic carbon.^{10, 11}

As of Figure S9, the precipitated HTs derived catalyst, a weight loss due to oxidation of carbon at higher temperature ranges was not observed. This demonstrates that the hydrotalcite derived catalyst Ni-Fe/Mg/Al (Fe/Ni = 0.1) has profound effect on carbon tolerance during the CO₂ methanation. According to previous report, incorporation of MgO on Ni-based catalysts for CO₂ reforming of methane was found as a promising approach to suppress the deposition of carbon and get improved catalyst stability.¹¹ Therefore, the presence of MgO on the structured hydrotalcite derived catalyst was found to be advantageous for its carbon tolerance nature through the improved CO₂ adsorption and dissociation properties.

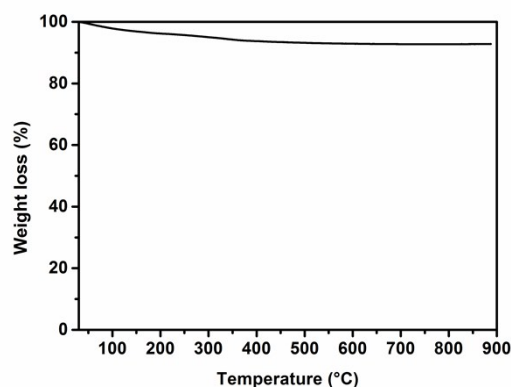


Figure S9 TG analysis of spent catalyst Ni-Fe/(Mg, Al)O_x (Fe/Ni = 0.1) HTs.

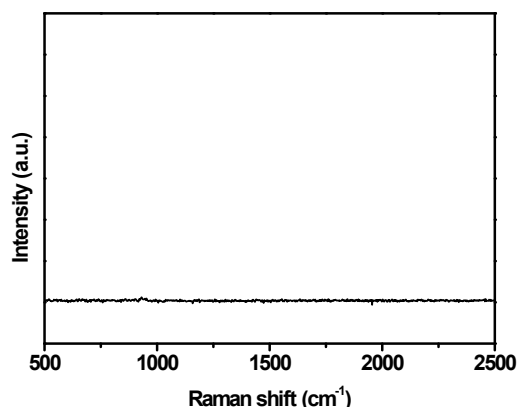


Figure S10 Raman spectrum of spent Ni-Fe/(Mg, Al)O_x (Fe/Ni = 0.1) HTs catalyst.

Raman spectrum of spent catalyst

Raman spectroscopy was also used to deeply investigate the nature and type of carbon deposited on the spent catalysts. According to Raman spectrum obtained (Figure S10), no peaks were obtained for the spent Ni-Fe/Mg-Al-HTs catalyst during the Raman spectroscopic analysis which approves the carbon tolerance nature of the catalyst.

Hemispherical model

The used hemispherical model similar to Tada et al.¹¹ is based on a uniform volume and single particles size d . The total perimeter or the metal-support interface L_{tot} and the total metal surface area S_{tot} were calculated by multiplying the perimeter l (Eq. 3) or surface area s (Eq. 4) for one hemisphere times the total number of hemispheres n (Eq. 1 and 2). The total number of hemispheres (Eq. 5) can be derived from metal loading ω , volume of the metal v (Eq. 7) and the linearly interpolated density ρ (Eq. 8).

$$L_{tot} = n \cdot l \quad (1)$$

$$S_{tot} = n \cdot s \quad (2)$$

$$l = \pi \cdot d \quad (3)$$

$$s = \frac{\pi \cdot d^2}{2} \quad (4)$$

$$n = \frac{\omega}{v \cdot \rho} \quad (5)$$

$$l = \pi \cdot d \quad (6)$$

$$v = \frac{\pi \cdot d^3}{12} \quad (7)$$

$$\rho = \rho_{Ni} \cdot x_{Ni} + \rho_{Fe} \cdot x_{Fe} \quad (8)$$

$$\text{with } x_{Ni} + x_{Fe} = 1$$

References

- 1 L. He, Q. Q. Lin, Y. Liu and Y. Q. Huang, *J Energy Chem*, 2014, **23**, 587-592.
- 2 S. Abello, C. Berrueco and D. Montane, *Fuel*, 2013, **113**, 598-609.
- 3 S. Hwang, J. Lee, U. G. Hong, J. C. Jung, D. J. Koh, H. Lim, C. Byun and I. K. Song, *J Ind Eng Chem*, 2012, **18**, 243-248.
- 4 G. Lee, Y. Jeong, A. Takagaki and J. C. Jung, *Journal of Molecular Catalysis A: Chemical*, 2014, **393**, 289-295.
- 5 I. Delidovich and R. Palkovits, *J Catal*, 2015, **327**, 1-9.
- 6 J. I. Di Cosimo, V. K. Diez, M. Xu, E. Iglesia and C. R. Apesteguia, *J Catal*, 1998, **178**, 499-510.
- 7 L. Chen, H. Dai, Y. Shen and J. Bai, *Journal of Alloys and Compounds*, 2010, **491**, L33-L38.
- 8 G. C. Allen, S. J. Harris, J. A. Jutson and J. M. Dyke, *Appl Surf Sci*, 1989, **37**, 111-134.
- 9 L. Bian, W. Wang, R. Xia and Z. Li, *Rsc Adv*, 2016, **6**, 677-686.
- 10 K. Y. Koo, H.-S. Roh, Y. T. Seo, D. J. Seo, W. L. Yoon and S. B. Park, *Applied Catalysis A: General*, 2008, **340**, 183-190.
- 11 S. Tada and R. Kikuchi, *Catal Sci Technol*, 2015, **5**, 3061-3070.